

Article

Influence of Calcination Temperature on Crystal Growth and Optical Characteristics of Eu³⁺ Doped ZnO/Zn₂SiO₄ Composites Fabricated via Simple Thermal Treatment Method

Suhail Huzaifa Jaafar ¹, Mohd Hafiz Mohd Zaid ^{1,2,*} , Khamirul Amin Matori ^{1,2}, Sidek Hj. Ab Aziz ¹, Halimah Mohamed Kamari ¹, Sawao Honda ³ and Yuji Iwamoto ³ 

¹ Department of Physics, Faculty of Science, Universiti Putra Malaysia, Serdang 43400 UPM, Selangor, Malaysia; suhailhuzaifa95@gmail.com (S.H.J.); khamirul@upm.edu.my (K.A.M.); sidek@upm.edu.my (S.H.A.A.); halimahmk@upm.edu.my (H.M.K.)

² Materials Synthesis and Characterization Laboratory, Institute of Advanced Technology, Universiti Putra Malaysia, Serdang 43400 UPM, Selangor, Malaysia

³ Department of Life Science and Applied Chemistry, Nagoya Institute of Technology, Gokisocho, Showaku, Nagoya 466-8555, Japan; honda@nitech.ac.jp (S.H.); iwamoto.yuji@nitech.ac.jp (Y.I.)

* Correspondence: mhmzaid@upm.edu.my

Abstract: This research paper proposes the usage of a simple thermal treatment method to synthesis the pure and Eu³⁺ doped ZnO/Zn₂SiO₄ based composites which undergo calcination process at different temperatures. The effect of calcination temperatures on the structural, morphological, and optical properties of ZnO/Zn₂SiO₄ based composites have been studied. The XRD analysis shows the existence of two major phases which are ZnO and Zn₂SiO₄ crystals and supported by the finding in the FT-IR. The FESEM micrograph further confirms the existence of both ZnO and Zn₂SiO₄ crystal phases, with progress in the calcination temperature around 700–800 °C which affects the existence of the necking-like shape particle. Absorption humps discovered through UV-Vis spectroscopy revealed that at the higher calcination temperature effects for higher absorption intensity while absorption bands can be seen at below 400 nm with dropping of absorption bands at 370–375 nm. Two types of band gap can be seen from the energy band gap analysis which occurs from ZnO crystal and Zn₂SiO₄ crystal progress. It is also discovered that for Eu³⁺ doped ZnO/Zn₂SiO₄ composites, the Zn₂SiO₄ crystal (5.11–4.71 eV) has a higher band gap compared to the ZnO crystal (3.271–4.07 eV). While, for the photoluminescence study, excited at 400 nm, the emission spectra of Eu³⁺ doped ZnO/Zn₂SiO₄ revealed higher emission intensity compared to pure ZnO/Zn₂SiO₄ with higher calcination temperature exhibit higher emission intensity at 615 nm with 700 °C being the optimum temperature. The emission spectra also show that the calcination temperature contributed to enhancing the emission intensity.

Keywords: thermal treatment; ZnO; Zn₂SiO₄; europium ion; composite



Citation: Jaafar, S.H.; Zaid, M.H.M.; Matori, K.A.; Aziz, S.H.A.; Mohamed Kamari, H.; Honda, S.; Iwamoto, Y. Influence of Calcination Temperature on Crystal Growth and Optical Characteristics of Eu³⁺ Doped ZnO/Zn₂SiO₄ Composites Fabricated via Simple Thermal Treatment Method. *Crystals* **2021**, *11*, 115. <https://doi.org/10.3390/cryst11020115>

Received: 3 January 2021

Accepted: 20 January 2021

Published: 26 January 2021

Publisher's Note: MDPI stays neutral with regard to jurisdictional claims in published maps and institutional affiliations.



Copyright: © 2021 by the authors. Licensee MDPI, Basel, Switzerland. This article is an open access article distributed under the terms and conditions of the Creative Commons Attribution (CC BY) license (<https://creativecommons.org/licenses/by/4.0/>).

1. Introduction

For the past decades, there has been a lot of studies regarding the luminescence material for the optical-electronic industry [1]. Luminescent materials such as phosphors are the substances that emit light in the electromagnetic waves (EM) spectrum after the conversion of the absorbed energy from an energy source. These materials may be classified according to the wide range of excitation energy sources and excitation trigger [2–4]. Essentially, photoluminescence is a phenomenon where the emission of light happens when stimulated by short-wavelength light, usually ultraviolet (UV) light or visible light [5]. Among many types of phosphors research, zinc silicate (Zn₂SiO₄) doped transition metal ions, as well as rare-earth ions have been one of the most popular host materials [6–8]. These numerous interests in zinc silicate phosphor also due to their interesting properties, having

good thermal and chemical stability [9], excel in water resistance with better resistance to nuclear radiation [10]. Zinc silicate also exhibits excellent luminescence properties when homogeneously grows with an inorganic oxide crystal [11–15].

In this work, zinc oxide (ZnO) crystal has been chosen as a crystal to be grown with zinc silicate (Zn_2SiO_4) crystal due to its ability to develop semiconductor material with huge direct transition allowed optical band gap energy (3.37 eV) [16] as well as high exciton binding energy (more than 60 meV) [17] added with exceptionally good thermal and chemical stability [18]. Therefore, ZnO crystal can be a proper application as a phosphor host in light-emitting diodes [19]. Several studies have been reported on the fabrication of ZnO/ Zn_2SiO_4 . The solid-state reaction had been used to fabricate ZnO/ Zn_2SiO_4 [20] with the fabricated sample showed broader visible range emissions compared to Zn_2SiO_4 and ZnO. Fabrication of ZnO/ Zn_2SiO_4 doped Eu^{3+} by sol-gel spin coating technique has also been reported [21]. PL study showed that the highest emission spectra obtained is around 610 nm which is at the red region due to the existence of Eu^{3+} ions in the sample and the emission intensity increased with the increment of calcination temperature. Recently, the Eu^{3+} ions are widely used as an energetic luminescent ion for the reason of its main sharp red emission at 615 nm, which results from the hypersensitive ($^5\text{D}_0 \rightarrow ^7\text{F}_2$) electronic dipole transition [22].

To fabricate pure and doped zinc silicate-based phosphor, various methods and techniques have been conducted. However, most of the fabrication techniques including solid-state reaction [23], sol-gel [24], and chemical methods [25] are hard to be utilized due to the high production cost. In addition, these methods are usually required high production energy with complex synthesis experimental techniques and often require long preparation time as well as a potentially environmental-harmful by-product. Hence, a novel developed simple reaction method has been applied to prepare Eu^{3+} doped $\text{Zn}_2\text{SiO}_4/\text{ZnO}$ composite due to the material handling simplicity, low energy consumption, and environmentally friendly [26]. The simple thermal treatment method has been used for the past few years to synthesis zinc selenide [27], $(\text{CuO})_{0.6}(\text{CeO}_2)_{0.4}$ [28], nickel ferrite nanocrystals [29], zinc oxide [30,31], and amorphous silica [32]. A simple thermal treatment method has also been used to fabricate ZnO-SiO₂ [33] and Zn_2SiO_4 by impregnating ZnO with amorphous SiO₂ [34].

The main objective of this research work is to study the effect of different calcination temperatures on morphological, optical, and photoluminescence properties of undoped and Eu^{3+} doped ZnO/ Zn_2SiO_4 composite synthesized via a simple thermal treatment method. The crystal growth, phase transformation, and microstructure of the composite samples were evaluated using XRD, FTIR, and FESEM micrograph. UV-visible absorbance and PL spectroscopy were used to evaluate the optical and photoluminescence properties of the composite samples. The excellent results in optical properties shown that the new composite samples can be proposed to be used as a red phosphor in optoelectronic applications. The novelty of this work is the usage of a new simple thermal treatment method to synthesis ZnO/ Zn_2SiO_4 and the introduction of Eu^{3+} ion as doping in the system.

2. Materials and Methods

2.1. Preparation of ZnO/ Zn_2SiO_4 Composite

To produce ZnO/ Zn_2SiO_4 based composites, the starting materials such as zinc acetate dihydrate as well as silicon tetraacetate was used as the precursors. The polyvinyl pyrrolidone (PVP) was added to the solution as the capping agent, for the purpose to reduce agglomeration and stabilize the composite particles. In this work, europium (III) acetate hydrate was used as a dopant. All the chemicals used were from Sigma Aldrich with 99.9% purity. Deionized water was used as a solvent. Firstly, 0.1 mmol (0.21951 g) of zinc acetate dihydrate (zinc source) followed by 0.1 mmol (0.26426 g) of silicon tetraacetate (silicon source) were added into an aqueous solution of 100 mL of deionized water. Next, 4 g of poly(vinyl) pyrrolidone (capping agent) was added to the solution. Then, 1 mol.% (0.003291 g) of europium (III) acetate hydrate which acts as the dopant was then added into

the solution and left for stirring for 2 h with the temperature of 80 °C to ensure the mixing of the solution [35]. The solution was then poured into petri dishes and left for drying in the oven at 120 °C for 24 h. After the drying process, the deposited residue which is yellow in colour at the wall of the dishes was scraped using a spatula and crushed into powder using pestle and mortar before heat-treated at different calcination temperatures; 600 °C, 700 °C, and 800 °C for 3 h.

2.2. Characterization

In this study, the undoped and Eu³⁺ doped ZnO/Zn₂SiO₄ samples undergo different analyses for structural, morphological, and optical properties of the samples. By employing X-ray diffraction (XRD) as well as Fourier-transform infrared spectroscopy (FTIR), structural properties of Eu³⁺ doped ZnO/Zn₂SiO₄ could be studied. The selected range of 2θ angles (degree) for the XRD analysis was specified within a Bragg angle (20°–80°). The crystalline phase of the samples was analyzed by utilizing the XRD machine from (Philips, Model: PW 3040/60 MPD X'PERT PRO PANalytical, Philips, Almelo, The Netherlands), with copper, Cu K_α radiation at 40 kV and 30 mA of the input current. The results were then examined using PANalytical X'Pert High Score software (PANalytical, Malvern, UK). While, for FTIR, these samples were analyzed using an FTIR spectrometer (Thermo Nicolet, Model: Nicolet 6700, Waltham, MA, USA) in the wavenumber range 200–4000 cm⁻¹. Field emission scanning electron microscopy (FESEM) was used to study the morphological behavior of Eu³⁺ doped ZnO-Zn₂SiO₄ samples. The specified properties of samples were viewed using (FEI, Model: Nova NanoSEM 230, Hillsboro, OR, USA) with 5 kV acceleration voltage. The gold coating was applied on top of the samples to prevent the charging effect from non-conductive specimens, with gold or platinum are usually chosen due to their thermal stability and the ability for a thin layer to form on the surface of the specimen.

For optical properties, ultraviolet-visible spectroscopy (UV-vis), band gap analysis, and photoluminescence (PL) analysis were used to analyze the Eu³⁺ doped ZnO/Zn₂SiO₄ samples. In this study, the absorbance of UV radiation was obtained through the diffuse reflectance technique using the UV/Vis/NIR spectrophotometer (SHIMADZU, Model: UV-3600, Kyoto, Japan). For optical band gap analysis, the model used was the Kubelka–Munk function which was proposed in 1931 by Kubelka and Munk [36]. By applying the Kubelka–Munk function, the measured reflectance spectra can be transformed to the corresponding absorption spectra as followed [37]:

$$F(R_{\infty}) = \frac{\alpha}{s} = \frac{(1 - R_{\infty})^2}{2R_{\infty}}, \quad (1)$$

where $R_{\infty} = \frac{R_{\text{sample}}}{R_{\text{standard}}}$ is the reflectance of an infinitely thick specimen, while α and s represent the absorption and scattering coefficients, respectively. Thus, the equation above could become

$$(F(R_{\infty}) \cdot hv)^{\frac{1}{\gamma}} = B(hv - E_g), \quad (2)$$

where h represents the Planck constant, ν represents the photon's frequency, E_g represents the optical band gap energy, and B represents the energy constant. The γ factor depends on the nature of the electron transition [38]. While for photoluminescence properties, the pure and Eu³⁺ doped ZnO/Zn₂SiO₄ based composites were analyzed using the photoluminescence spectrometer (PERKIN ELMER, Model: LS 55, Waltham, MA, USA). 350 nm was chosen as the excitation wavelength to study the effect of different calcination temperatures on photoluminescence properties of undoped samples while for Eu³⁺ doped ZnO/Zn₂SiO₄ based composites, 400 nm was chosen as the excitation wavelength.

3. Results and Discussion

3.1. X-ray Diffraction (XRD) Analysis

To study the crystalline substances present, the XRD test has been carried on the samples. Figure 1 shows the XRD finding of silicon tetraacetate, Si source for the samples.

The broad spectrum and absence of peaks indicates that the silicon tetraacetate is in amorphous state. Figure 1 also shows the XRD peak of zinc acetate which acts as the Zn source for the samples. The peaks available proposes the existence of ZnO crystals in zinc acetate. Figure 1 also present ZnO/Zn₂SiO₄ samples spectrum which undergoes calcination process with different temperatures; 600 °C, 700 °C, and 800 °C for 3 h. As can be seen from the graph, the pattern from 600 °C calcination temperature exhibits a handful of sharp peaks which suggests the crystallinity of the ZnO peaks which presents the existence of ZnO element in the samples. This corresponds with the findings from the previous study [25].

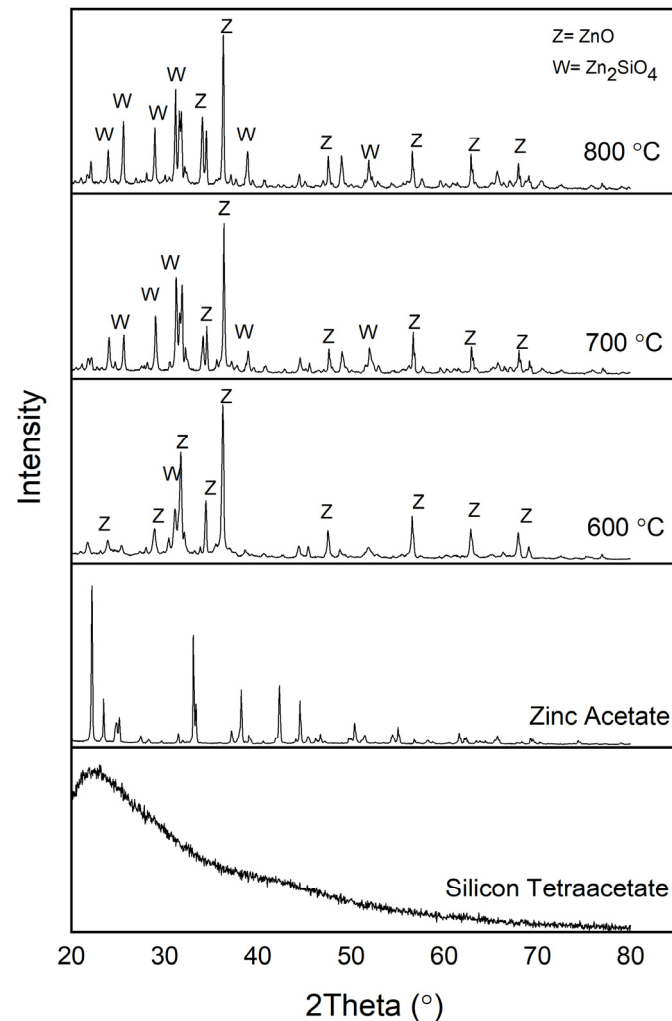


Figure 1. XRD spectrum of ZnO/Zn₂SiO₄ sample calcined at various temperatures for 3 h.

The existence of the Zn₂SiO₄ crystal peak can also be discovered at around 31.5° which shows the formation of Zn₂SiO₄ as ZnO and SiO₂ fused during the calcination process. While the XRD spectra of samples heat-treated at 700 °C show the diffraction patterns which belong to zinc silicate (Zn₂SiO₄) phases (JCPDS No. 37-1485) at 25°, 28°, 31.5°, 48°, and 56°. Several phases containing ZnO (JCPDS No. 36-1451) also can be seen in the spectra at 32°, 34°, 36.5°, 53°, 63°, and 68.5°. SiO₂ peaks at 24.5° and 28.7° are low and can almost be neglected. At this calcination temperature, the intensity of the ZnO peak at 36.5° is higher than the Zn₂SiO₄ peak at 31.5°. It is also found that at this calcination temperature, the number of ZnO peaks decreased while the amount of Zn₂SiO₄ peaks increased compared to the lower temperature. This is due to the higher energy provided during the calcination process which led to high surface mobility of Zn and Si ions for the formation of Zn₂SiO₄ in the samples [39]. As the calcination temperature progressed further

to 800 °C, the intensity of the Zn_2SiO_4 peaks at 28° and 31.5° increased which indicates that the increment of calcination temperatures will affect better crystallization process which will also lead to the increment of the diffraction peak intensity [40–42]. By further observing the graph, the diffraction peak sharpness tends to increase with the increment of calcination temperatures with the full width at half maxima (FWHM) value become lower which decrease from 0.2273 to 0.1624. Usually smaller FWHM means the progress of larger particle size. This is because the enhancement of the crystallization process in the samples will leads to a sharper diffraction peak. Based on the previous report, the rate of ions diffusion in the samples increases at higher calcination temperature which accelerates the crystal's growth rate and produces larger crystals size in the samples [43]. From Figure 2, not many differences can be seen in the spectrum pattern of the Eu^{3+} doped $\text{ZnO}/\text{Zn}_2\text{SiO}_4$ as compared to the undoped spectrum. However, at the calcination temperature of 700 °C, the intensity of the Zn_2SiO_4 peak at 31.5° is higher than the ZnO peak at 36.5°. This shows that at this temperature, the addition of Eu^{3+} in the sample may help for the formation of Zn_2SiO_4 in the samples; however, further increasing the calcination temperature may affect the diffraction peak of Zn_2SiO_4 to become lower due to the possibility of lattice distortion in the structural system in the samples [44]. From Figure 2, it is also observed that there are no Eu_2O_3 peaks or any other peak besides ZnO and Zn_2SiO_4 can be seen in the graph indicated that the dopant was well dissolved in the $\text{ZnO}/\text{Zn}_2\text{SiO}_4$ crystal lattice.

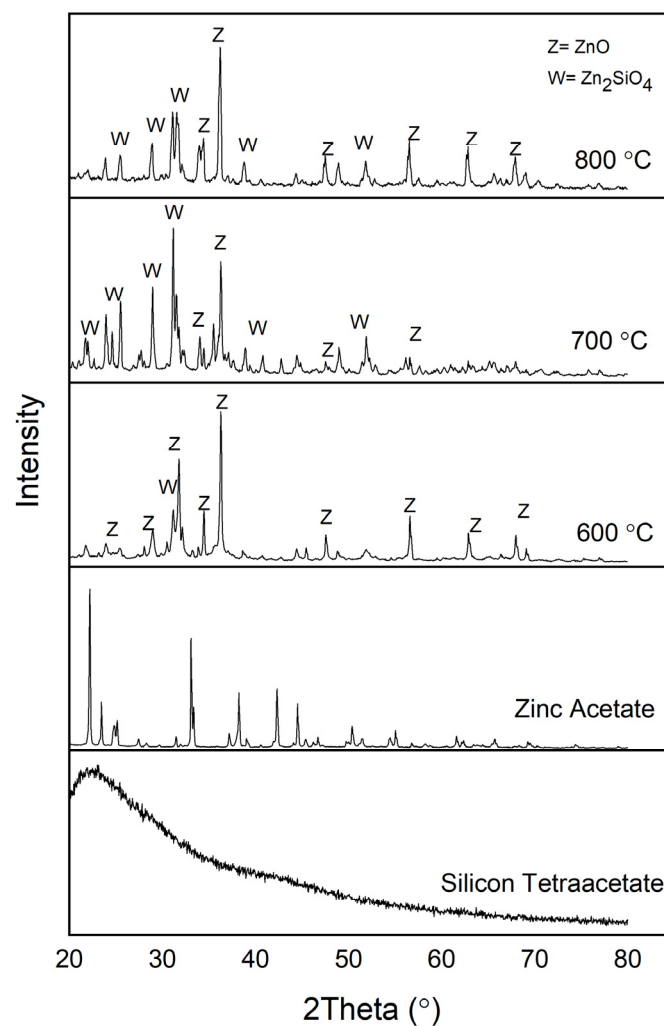


Figure 2. XRD spectrum of Eu^{3+} doped $\text{ZnO}/\text{Zn}_2\text{SiO}_4$ composites calcined at different temperatures for 3 h.

3.2. Fourier Transform Infrared (FT-IR) Spectroscopy

To study the functional group and the phase composition of the ZnO/Zn₂SiO₄ samples after the calcination process, FT-IR spectroscopy was used. Figures 3 and 4 below show the spectra for the functional group and phase composition of the undoped and Eu³⁺ doped ZnO/Zn₂SiO₄ based composites respectively, which undergo different calcination temperatures which are 600, 700, and 800 °C for 3 h. The main peaks of the compounds in the spectra fall in the frequency range of 400–2500 cm⁻¹. Essentially, both figures show the same pattern where, the spectrum display absorption peaks at 462, 500, 580, 620, 700, 802, 884, 989, 1002, and 1100 cm⁻¹. The absorption peak at a wavenumber of 462, 500, and 580 cm⁻¹ indicated the symmetric stretching vibration of the ZnO₄ group [21,38,41,45]. Absorption peaks present at 620 and 700 cm⁻¹ ascribed to the ZnO₄ asymmetric stretching and SiO torsional vibrations whereas peaks at 812 and 884 cm⁻¹ were assigned to the SiO₄ symmetric stretching vibration [21,38,41,42,45,46]. The absorption peak around 989 cm⁻¹ was assigned to the SiO₄ asymmetric stretching vibration [15,45,47]. The existence of the vibrations of SiO₄ and ZnO₄ groups being evidence of the formation of the Zn₂SiO₄ phase [47–49]. The vibrational band observed at 1110 cm⁻¹ ascribed to the Si-O-Si asymmetric stretching vibrations [15,20]. From the Figures 3 and 4, it is found that the increment in the absorption peak intensity at 580 cm⁻¹ which implied the enhancement of ZnO₄ group unit by replacing the Si atoms [48]. Next, from the same figures, the dropping in the peak intensity at 620 and 1110 cm⁻¹ can be seen which indicates the decrement of the asymmetrical stretching of ZnO₄ and Si-O-Si due to the breaking of ZnO₄ and Si-O-Si bonds during the formation of Zn₂SiO₄ [49]. Table 1 further simplified the absorption band and the corresponding assignment band of the ZnO/Zn₂SiO₄ composites. The absence of the peaks in the range of 2000–2500 cm⁻¹ in the spectrum indicates that there are no C-O mode and C-H stretching mode of organic sources [29]. With the increase in the calcination temperature, the spectrum shifts slightly to the lower wavelength in the vibrational bands which favors ZnO/Zn₂SiO₄ composites crystallization and formation [45]. The addition of Eu³⁺ in the sample may not affect much to the pattern, as a similar pattern can be seen for both figures.

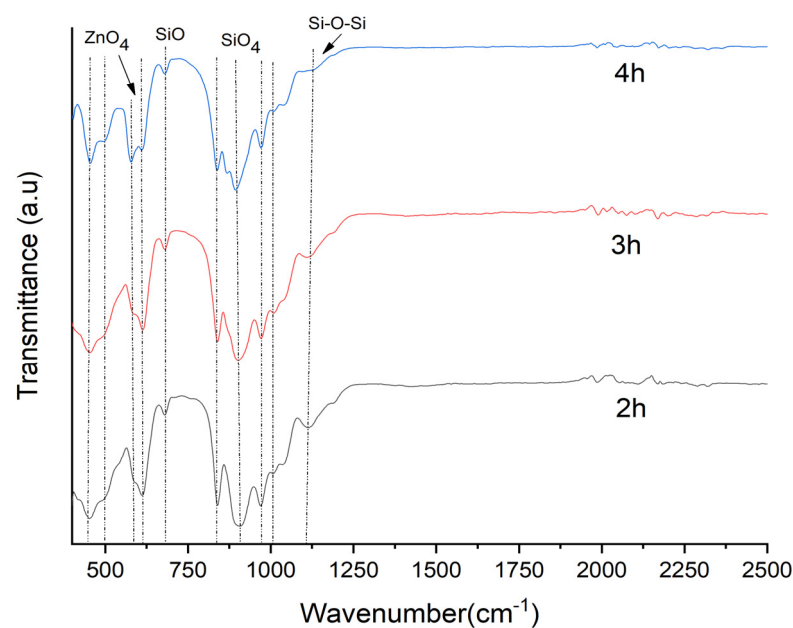


Figure 3. FT-IR spectra of ZnO/Zn₂SiO₄ composites calcined at different temperatures (°C) for 3 h.

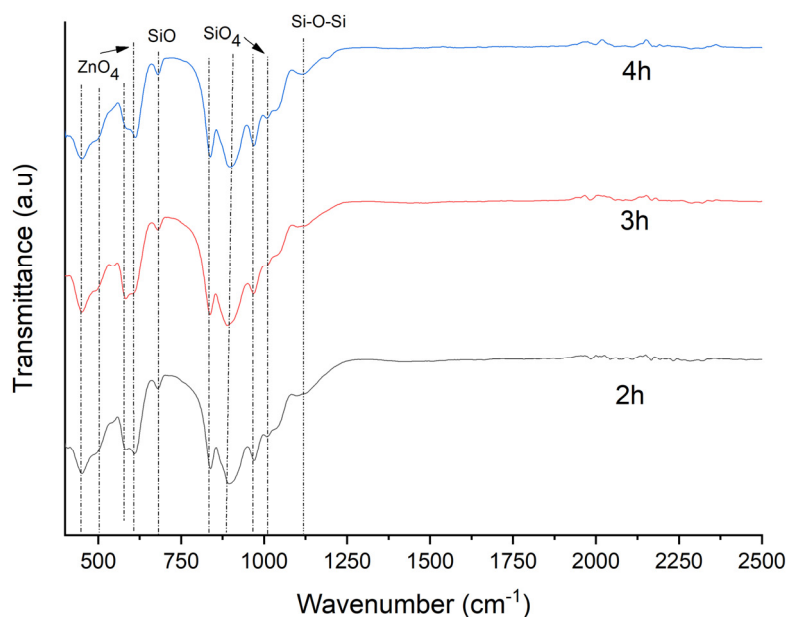


Figure 4. FT-IR spectra of Eu^{3+} doped $\text{ZnO}/\text{Zn}_2\text{SiO}_4$ composites calcined at different temperatures ($^\circ\text{C}$) for 3 h.

Table 1. FT-IR absorption bands and the corresponding assignment bands of $\text{ZnO}/\text{Zn}_2\text{SiO}_4$ composites.

Wavenumber (cm^{-1})	Assignment of Vibrational Mode	Reference(s)
462–580	ZnO_4 symmetric stretching vibration	[21,38,41]
620	ZnO_4 asymmetric stretching vibration	[21,41,42,46]
700	SiO torsional vibrations	[41]
812–884	SiO_4 symmetric stretching vibration	[38,42,45–47]
989	SiO_4 asymmetric stretching vibration	[15,45,47]
1100	Si-O-Si asymmetric stretching vibration	[15,20]

3.3. Field Emission Scanning Electron Microscope (FESEM) Analysis

To understand the characteristics of the surface morphology and elemental composition of $\text{ZnO}/\text{Zn}_2\text{SiO}_4$ based composites, FESEM analysis has been done. Below are the figures for FESEM images of pure and Eu^{3+} doped $\text{ZnO}/\text{Zn}_2\text{SiO}_4$ based composites heat-treated at various calcination temperatures at 3 h holding time. Figure 5a shows the separated tiny particles in the structure in the sample at 600°C of calcination temperature. As the calcination temperature increased, the surface energy in the samples also tends to become higher which caused smaller particles to fuse with the neighboring particles thus, forming larger crystallite sizes [50–52]. From Figure 5c, the existence of several necking-like shape particles can be seen in the sample with 800°C calcination temperature. For Eu^{3+} doped $\text{ZnO}/\text{Zn}_2\text{SiO}_4$ based composites, a similar pattern can be seen. As the calcination temperature progresses further to 800°C , a lot of dumbbell-like structures can be seen with a higher particle size as in Figure 5f. This is maybe due to the effect of the agglomeration of neighboring particles by further increasing the calcination temperature which will enhance the diffusion between particles by melting their surfaces, thus forming the dumbbell-like structure in the sample [25].

3.4. Ultraviolet-Visible Spectroscopy (UV-Vis)

The effects of calcination temperatures on the optical properties, specifically the light absorption characteristic of $\text{ZnO}/\text{Zn}_2\text{SiO}_4$ samples has been studied by undergoing the Ultraviolet-visible spectroscopy (UV-vis) in the UV-visible range of 250–800 nm. The below figures show the absorption spectrum of pure and Eu^{3+} doped $\text{ZnO}/\text{Zn}_2\text{SiO}_4$ based composites undergo different calcination temperatures, which are 600°C , 700°C , and

800 °C for 3 h. Figure 6 shows the absorption spectra of undoped ZnO/Zn₂SiO₄ with different calcination temperatures for 3 h. From the graph, it is observed that undoped ZnO/Zn₂SiO₄ has an absorption band of below 400 nm with higher calcination temperature contributed to higher absorption intensity. This happened due to the scattering of Zn₂SiO₄ crystals in the samples [53,54]. The absorption bands displayed the red-shift pattern due to the process of crystallization during the calcination process. Dropping of absorption edge also can be seen around 370 nm, which due to the possibility of ZnO structure collapse thus formed the Zn₂SiO₄ structure [54]. By observing Figure 7, the absorption spectrum of Eu³⁺ doped ZnO/Zn₂SiO₄ shows quite a similar pattern to those of undoped samples, with an absorption band of below 400 nm. The absorption spectrum of the doped ZnO/Zn₂SiO₄ shows that the absorption band is having red-shift as the calcination temperature increased, due to the enhancement of crystallization in the samples which also show that the absorption edge has been enhanced. The UV-vis spectrum of Eu³⁺ doped ZnO/Zn₂SiO₄ also show the pattern of higher calcination temperature affect to higher absorption intensity, due to the scattering of Zn₂SiO₄ crystals in the samples while, the dropping of absorption edge can be seen at around 375 nm, thanks to the reason of ZnO structure collapse which formed the Zn₂SiO₄ structure, as associated with XRD findings.

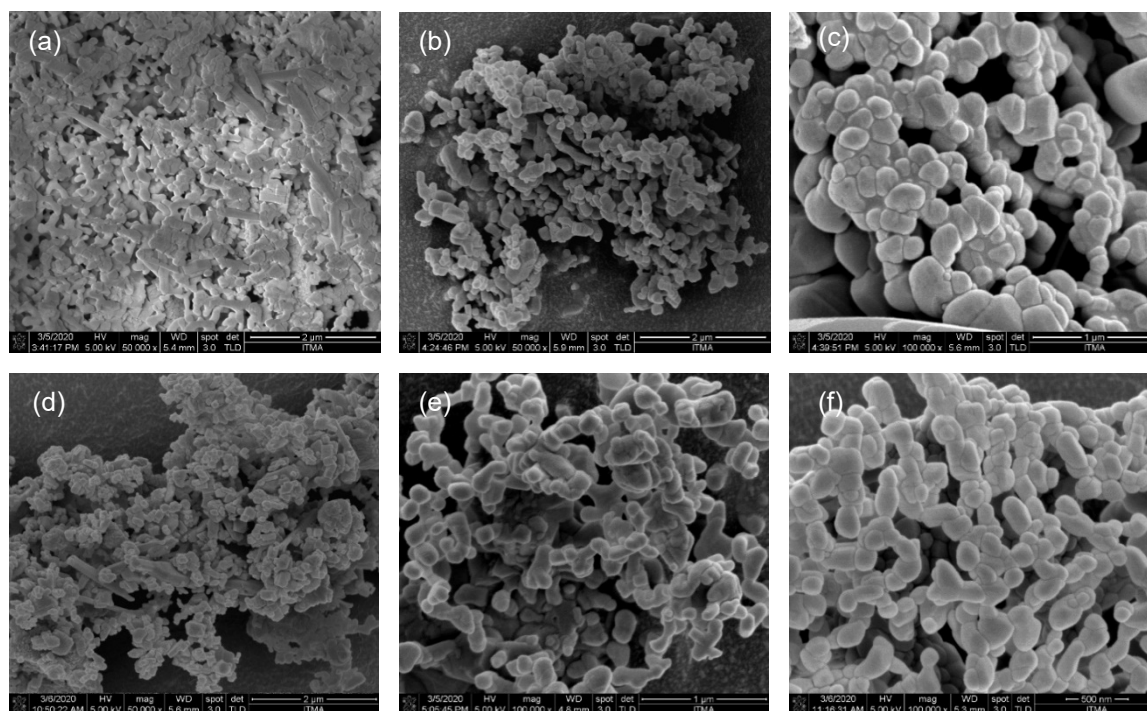


Figure 5. FESEM images of ZnO/Zn₂SiO₄ calcined for 3 h with (a) 0% Eu³⁺ at 600 °C, (b) 0% Eu³⁺ at 700 °C, (c) 0% Eu³⁺ at 800 °C, (d) 1% Eu³⁺ at 600 °C, (e) 1% Eu³⁺ at 700 °C, (f) 1% Eu³⁺ at 800 °C.

3.5. Optical Band Gap Analysis

The effect of calcination temperature on the optical band gap energy (E_g) of ZnO/Zn₂SiO₄ synthesized between 600 and 800 °C was determined by applying the Kubelka–Munk function using diffuse reflectance technique. The γ factor value used is $\gamma = 1/2$, which is a direct allowed transition. The figures below show the optical band gap spectra of pure and Eu³⁺ doped ZnO/Zn₂SiO₄ based composites undergo different calcination temperatures which are 600, 700, and 800 °C for 3 h. Essentially, two different band gap values were observed and calculated for each ZnO/Zn₂SiO₄ composite sample. This is due to the existence of two phases in the composite, which is the ZnO phase and Zn₂SiO₄ crystal phase, under XRD and FESEM findings.

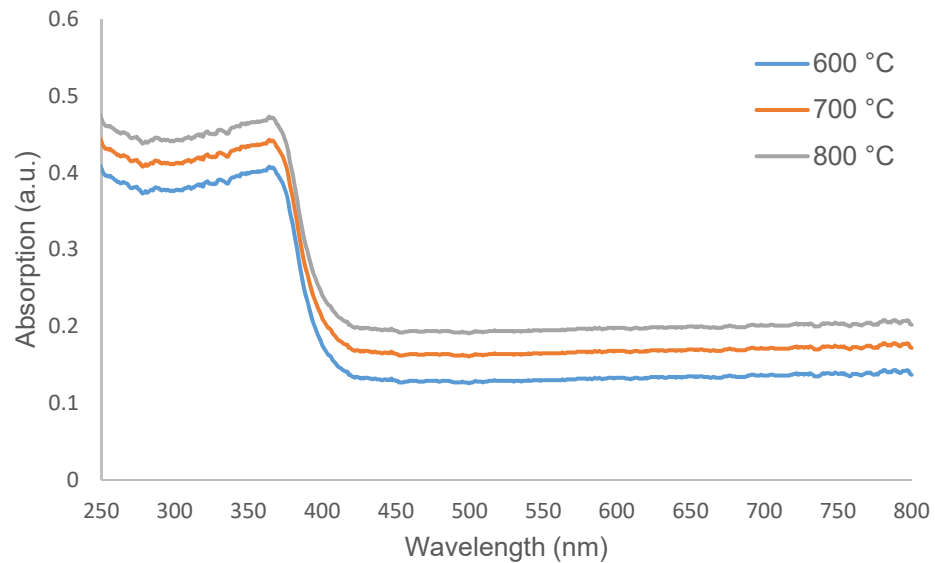


Figure 6. UV-vis absorption spectra of ZnO/Zn₂SiO₄ composites calcined at different temperatures (°C) for 3 h.

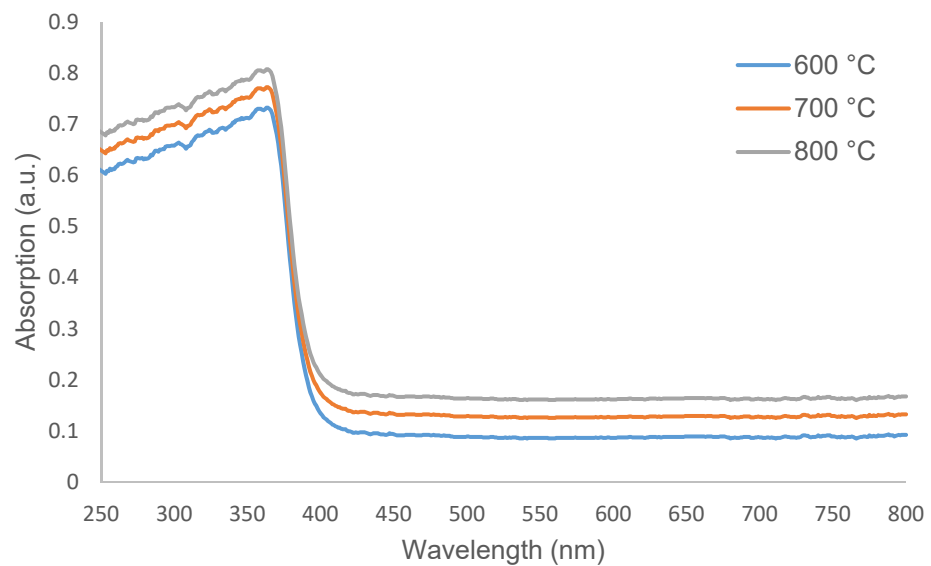


Figure 7. UV-vis absorption spectra of Eu³⁺ doped ZnO/Zn₂SiO₄ composites calcined at different temperatures (°C) for 3 h.

From Figure 8, the direct energy band gap value of the undoped ZnO/Zn₂SiO₄ observed by extrapolating the linear portion of the optical absorption plot is between 3.21 and 3.17 eV for ZnO crystal and 5.21 to 4.09 eV for Zn₂SiO₄ crystal which are tabulated in Table 2. It is observed that for both the crystals phase, the optical band gap value produced is decreasing with the increment of calcination temperature. This is due to higher calcination temperature will induce a red-shift of the electronic absorption edge, producing a smaller energy band gap which is associated with the crystallization process in the sample [50,55]. While, for Eu³⁺ doped ZnO/Zn₂SiO₄ composite samples, Figure 9 shows that the energy band gap value of ZnO crystal increased (3.271–4.07 eV) as the calcination temperature increased. This is maybe due to the possibility of ZnO crystals became deteriorated as the calcination temperature became higher [56]. However, the energy band gap value of Zn₂SiO₄ crystal is decreasing (5.11–4.71 eV) as the calcination temperature increases. This is caused by the crystallization process that occurred in the

sample which produces a smaller energy band gap hence affect the occurrence of red-shift patterns in the sample [55].

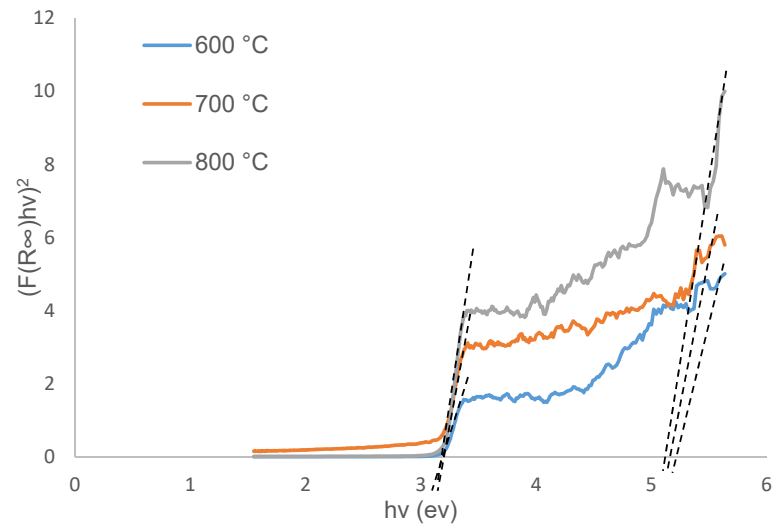


Figure 8. Plot of $(F(R_{\infty})hv)^2$ against hv of ZnO/Zn₂SiO₄ composites calcined at different temperatures (°C) for 3 h.

Table 2. Optical band gap energy (E_g) value for undoped and Eu³⁺ doped ZnO/Zn₂SiO₄ composites.

Sample	Calcination Temperature (°C)	ZnO E_g (eV)	Zn ₂ SiO ₄ E_g (eV)
undoped	600 °C	3.21	5.21
undoped	700 °C	3.19	5.18
undoped	800 °C	3.17	5.09
Eu ³⁺ doped	600 °C	3.27	5.11
Eu ³⁺ doped	700 °C	3.68	4.93
Eu ³⁺ doped	800 °C	4.07	4.71

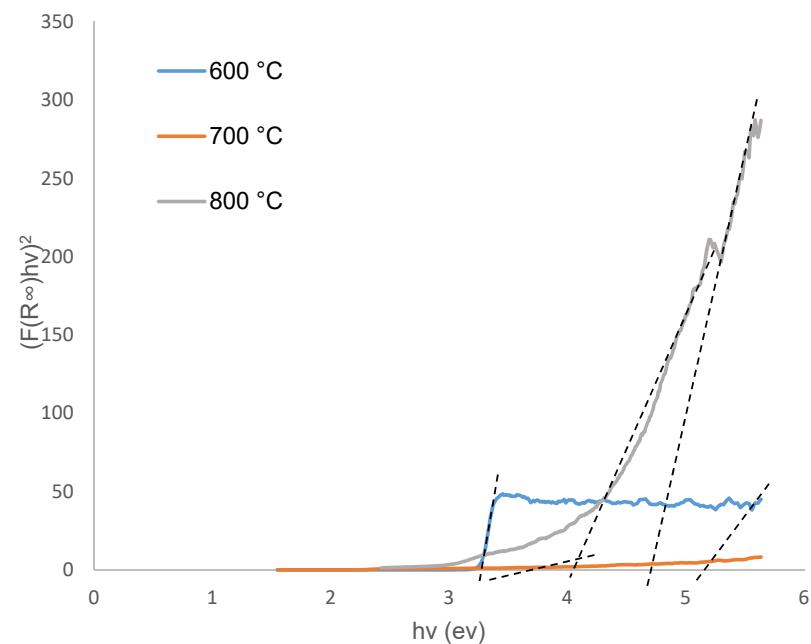


Figure 9. Plot of $(F(R_{\infty})hv)^2$ against hv of Eu³⁺ doped ZnO/Zn₂SiO₄ composites calcined at different temperatures (°C) for 3 h.

3.6. Photoluminescence (PL) Analysis

PL analysis was done to study and understand the photoluminescence properties of undoped and Eu^{3+} doped $\text{ZnO}/\text{Zn}_2\text{SiO}_4$ composite samples. The measured emission spectra of the $\text{ZnO}/\text{Zn}_2\text{SiO}_4$ samples are between 450 and 700 nm. Figure 10 shows the emission spectra of undoped $\text{ZnO}/\text{Zn}_2\text{SiO}_4$ based composites excited under 350 nm while Figure 11 shows Eu^{3+} doped $\text{ZnO}/\text{Zn}_2\text{SiO}_4$ samples excited under 400 nm [57]. From Figure 10, several emission peaks can be seen at 460, 485, and 575 nm which are associated with violet-blue, blue, and green regions, respectively. The emission peak at around 460 nm is indicated to the transition of an electron from Zn interstitial to the valence band and from conduction band to oxygen defects in the region of violet-blue and commonly referred to as blue emission while at the emission wavelength of 485 nm, the peak is associated to the zinc interstitials [57,58]. Located within the green region, the emission peak of 575 nm was associated with the transition of electrons between the valence band and conduction band [56]. From the same figures, it is also observed that as the calcination temperature increases from 600 °C to 700 °C, the emission peaks also increases. This is due to the enhancement of the crystal quality in the material [59].

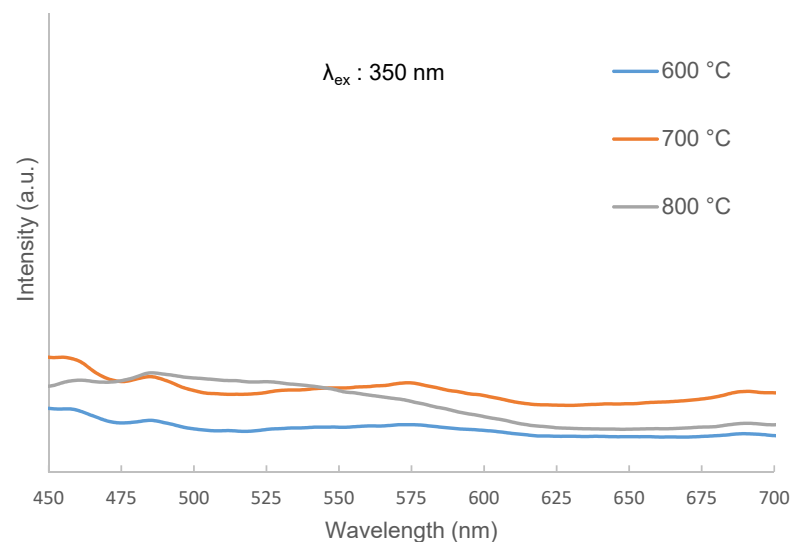


Figure 10. Photoluminescence (PL) spectra of $\text{ZnO}/\text{Zn}_2\text{SiO}_4$ composites calcined at different temperatures (°C) for 3 h.

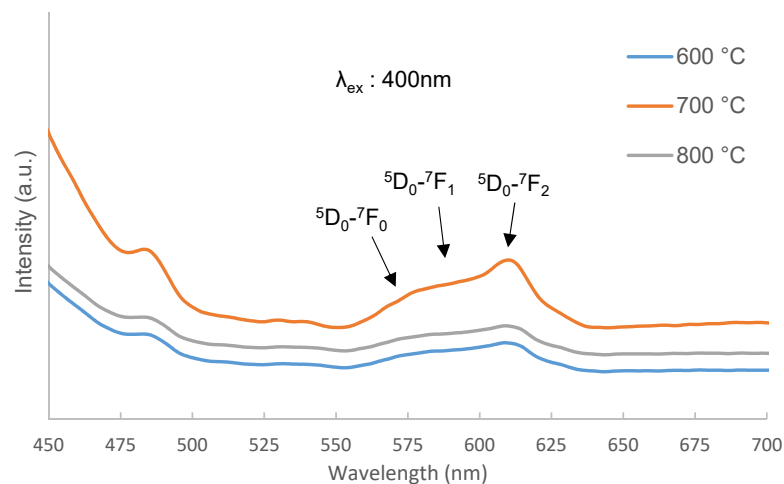


Figure 11. PL spectra of Eu^{3+} doped $\text{ZnO}/\text{Zn}_2\text{SiO}_4$ composites calcined at different temperatures (°C) for 3 h.

For the Eu^{3+} doped $\text{ZnO}/\text{Zn}_2\text{SiO}_4$, Figure 11 shows three major emission peaks in the emission spectra which are at 578, 590, and 615 nm, attributed to the electronic transitions ${}^5\text{D}_0 \rightarrow {}^7\text{F}_0$, ${}^5\text{D}_0 \rightarrow {}^7\text{F}_1$, and ${}^5\text{D}_0 \rightarrow {}^7\text{F}_2$ of Eu^{3+} ion, respectively [21]. However, before that, the broad emission peak at 485 nm can be related to the transition from the ionized oxygen vacancies to the valence band [60]. The blue-green emission peak can be due to the transition of an electron from interstitial zinc to zinc vacancies or interstitial oxygen as well as the transition originated from a complex defect level of oxygen vacancies and interstitial zinc to the valence band. The red-shift of the peak is mainly due to the unlike crystalline phases between the samples and thus the different host crystal field. Generally, during the heat-treatment process, the formation of ZnO and Zn_2SiO_4 crystals may affect the local environment of Eu^{3+} ions, which indicate that Eu^{3+} ions may be incorporated both into the ZnO and Zn_2SiO_4 lattice where the coordination number of Eu^{3+} may intensely influence the emission color of the ZnO and Zn_2SiO_4 crystal lattice to produce red emission color [21]. This can be discovered from FESEM images, where no Eu^{3+} structure can be seen in the images regardless of the concentration of Eu^{3+} , which shows that Eu^{3+} has been incorporated into both crystals sites.

Next, the ${}^5\text{D}_0 \rightarrow {}^7\text{F}_0$ transition at the emission peak of 578 nm belongs to the 4f-4f transitions, which is principally forbidden according to the standard selection rules of the Judd–Ofelt theory [61]. Hence, the peak should be inexistent or very weak in the PL emission spectrum, however, due to the possibility of the majority of Eu^{3+} ions occupy the interstitial sites with much lower local symmetry in the $\text{ZnO}/\text{Zn}_2\text{SiO}_4$ host, hence affect to the occurrence of ${}^5\text{D}_0 \rightarrow {}^7\text{F}_0$ transition [62,63]. While the emission peak at 590 nm with the electronic transitions ${}^5\text{D}_0 \rightarrow {}^7\text{F}_1$ is attributed to the magnetic allowed transitions ($\Delta j = 1$) with an insensitive magnetic dipole transition to the environment [21,64,65]. As shown in the figure, the prominent emission peak is found at 615 nm with the electronic transitions ${}^5\text{D}_0 \rightarrow {}^7\text{F}_2$. This transition is ascribed to the allowed transitions of an electric dipole ($\Delta j = 2$) with hypersensitive electric dipole transition to the crystal field environment [21,66]. At 615 nm, the strong emission peak of Eu^{3+} which is characteristically red emission was attributed to magnetic dipole (MD) transitions. This peak shows that the Eu^{3+} ions had occupied the non-centrosymmetric site in the Zn_2SiO_4 crystal lattice [67]. The peak in the emission spectra was also almost similar to the emission peak of the commercial red phosphors ($\text{Y}_2\text{O}_3:\text{Eu}$ from Nichia Corporation, Japan) which show that the highest emission peak is around 615 nm, which support the emission peak of this work having the highest emission peak at 615 nm [68]. From the graph, it was also shown that the 700 °C samples produced higher emission peaks as compared to 600 °C and 800 °C. This shows that 700 °C was the optimum calcination temperature for the red emission and will emit the brightest red color when excited under the UV lamp.

4. Conclusions

Eu^{3+} doped $\text{ZnO}/\text{Zn}_2\text{SiO}_4$ based composite has been successfully fabricated using the simple thermal treatment method. The XRD results confirmed the existence of two crystal phases; ZnO phase and Zn_2SiO_4 phase with the highest peak at 36.5° (ZnO) and 31.5° (Zn_2SiO_4), supported by FT-IR and FESEM. Eu^{3+} doped $\text{ZnO}/\text{Zn}_2\text{SiO}_4$ calcined at 700 °C showed higher Zn_2SiO_4 peak (31.5°) compared to ZnO peak (36.5°) and further increment of calcination temperature may cause the Zn_2SiO_4 peaks to drop due to the lattice distortion occurred. FESEM micrograph suggested that increment in the calcination temperature may affect to the existence of dumbbell-like structures to appear in the sample, indicates that the agglomeration of neighboring particles happen in the composite. Next, absorption band intensity tend to become higher as calcination temperature increased. Furthermore, the crystallization process during calcination had affected the occurrence of red shift in the absorption spectra. Eu^{3+} doped $\text{ZnO}/\text{Zn}_2\text{SiO}_4$ based composite also possessed two band gap energy which are ZnO crystal E_g value (3.271 to 4.07 eV) and Zn_2SiO_4 crystal E_g value (5.11 to 4.71 eV). The E_g value for Zn_2SiO_4 crystal calculated become lower with increment of calcination temperature. PL study showed that Eu^{3+} doped $\text{ZnO}/\text{Zn}_2\text{SiO}_4$ calcined at 700 °C is the optimum condition for red phosphor by

emitting the highest emission intensity at ~615 nm. We believed the fabricated Eu^{3+} doped $\text{ZnO}/\text{Zn}_2\text{SiO}_4$ via simple thermal treatment method are suitable to be used for red phosphor for several applications such as LEDs for its good emission intensity in the red region and the simplicity of the technique. In the presented work, the structural, morphological, and optical properties of Eu^{3+} doped $\text{ZnO}/\text{Zn}_2\text{SiO}_4$ composites has been presented. However, the thermal and electrochemical properties of the material need to be studied and verified in the future.

Author Contributions: Conceptualization, S.H.J., M.H.M.Z., K.A.M., and S.H.A.A.; methodology, S.H.J., M.H.M.Z., K.A.M. and S.H.A.A.; software, S.H.J., M.H.M.Z., S.H. and Y.I.; validation, S.H.J., M.H.M.Z., and K.A.M.; formal analysis, S.H.J., M.H.M.Z., K.A.M., S.H., and Y.I.; investigation, S.H.J., M.H.M.Z., K.A.M., S.H.A.A. and H.M.K.; resources, K.A.M., S.H.A.A., H.M.K., S.H. and Y.I.; data curation, S.H.J. and M.H.M.Z.; writing—original draft preparation, S.H.J., M.H.M.Z., K.A.M. and S.H.A.A.; writing—review and editing, M.H.M.Z., H.M.K., S.H., and Y.I.; visualization, S.H.J.; supervision, M.H.M.Z., K.A.M. and H.M.K.; project administration, M.H.M.Z.; funding acquisition, M.H.M.Z. All authors have read and agreed to the published version of the manuscript.

Funding: The financial support from the Universiti Putra Malaysia (UPM) under the Putra Research Grant was gratefully acknowledged.

Data Availability Statement: Data is contained within the article.

Acknowledgments: Authors would like to thank Yuji Iwamoto, Japan, for measurement as well as for their general cooperation during the project.

Conflicts of Interest: The authors declare no conflict of interest. The funders had no role in the design of the study; in the collection, analyses, or interpretation of data; in the writing of the manuscript, or in the decision to publish the results.

References

1. Luo, X.X.; Cao, W.H. Upconversion luminescence of holmium and ytterbium co-doped yttrium oxysulfide phosphor. *Mater. Lett.* **2007**, *61*, 3696–3700. [[CrossRef](#)]
2. Wu, Z.; Mo, S.; Tan, L.; Fang, B.; Su, Z.; Zhang, Y.; Yin, M. Crystallization-Induced Emission Enhancement of a Deep-Blue Luminescence Material with Tunable Mechano-and Thermochromism. *Small* **2018**, *14*, 1802524. [[CrossRef](#)] [[PubMed](#)]
3. Edgar, A. Luminescent Materials. In *Springer Handbook of Electronic and Photonic Materials*; Kasap, S., Capper, P., Eds.; Springer International Publishing: Cham, Switzerland, 2017; p. 1.
4. Rojas-Hernandez, R.E.; Rubio-Marcos, F.; Rodriguez, M.Á.; Fernandez, J.F. Long lasting phosphors: SrAl_2O_4 : Eu, Dy as the most studied material. *Renew. Sustain. Energy Rev.* **2018**, *81*, 2759–2770. [[CrossRef](#)]
5. Shionoya, S. Photoluminescence. In *Luminescence of Solids*; Vij, D.R., Ed.; Springer: Boston, MA, USA, 1998; pp. 95–133.
6. Khaidir, R.E.M.; Fen, Y.W.; Zaid, M.H.M.; Matori, K.A.; Omar, N.A.S.; Anuar, M.F.; Wahab, S.A.A.; Azman, A.Z.K. Optical band gap and photoluminescence studies of Eu^{3+} -doped zinc silicate derived from waste rice husks. *Optik* **2019**, *182*, 486–495. [[CrossRef](#)]
7. Effendy, N.; Kamari, H.M.; Zaid, M.H.M.; Liew, J.Y.C.; Lee, H.K.; Rahman, N.A.A.; Wahab, S.A.A.; Khiri, W.Z.A.; El-Mallawany, R. Synthesis and green luminescence of low cost Er_2O_3 doped zinc silicate glass-ceramics as laser materials. *Optik* **2019**, *184*, 480–484. [[CrossRef](#)]
8. Rasdi, N.M.; Fen, Y.W.; Omar, N.A.S. Photoluminescence studies of cobalt (II) doped zinc silicate nanophosphors prepared via sol-gel method. *Optik* **2017**, *149*, 409–415. [[CrossRef](#)]
9. Yang, R.Y.; Peng, Y.M.; Lai, H.L.; Chu, C.J.; Chiou, B.; Su, Y.K. Effect of the different concentrations of Eu^{3+} ions on the microstructure and photoluminescent properties of Zn_2SiO_4 : $x\text{Eu}^{3+}$ phosphors and synthesized with TEOS solution as silicate source. *Opt. Mater.* **2013**, *35*, 1719–1723. [[CrossRef](#)]
10. He, Y.; Zhao, X.; Wang, X.; Chen, L.; Peng, W.; Ouyang, X. Characterizations of an X-ray detector based on a Zn_2SiO_4 film. *Sens. Actuator A Phys.* **2015**, *236*, 98–103. [[CrossRef](#)]
11. Chelouche, A.; Djouadi, D.; Aksas, A. Structural characterization of $\text{SiO}_2/\text{Zn}_2\text{SiO}_4$: Ce nanocomposite obtained by sol gel method. *J. Assoc. Arab Univ. Basic Appl. Sci.* **2014**, *15*, 10–14. [[CrossRef](#)]
12. Ramakrishna, P.V.; Murthy, D.B.R.K.; Sastry, D.L.; Samatha, K. Synthesis, structural and luminescence properties of Mn doped $\text{ZnO}/\text{Zn}_2\text{SiO}_4$ composite microphosphor. *Spectrochim. Acta A Mol. Biomol. Spectrosc.* **2014**, *129*, 274–279. [[CrossRef](#)]
13. Mbule, P.S.; Ntwaeaborwa, O.M.; Mothudi, B.M.; Dhlamini, M.S. Structural and optical characterization of nanoparticulate manganese doped zinc silicate phosphors prepared by sol-gel and combustion methods. *J. Lumin.* **2016**, *179*, 74–82. [[CrossRef](#)]
14. Omar, N.A.S.; Fen, Y.W.; Matori, K.A.; Zaid, M.H.M.; Samsudin, N.F. Structural and optical properties of Eu^{3+} activated low cost zinc soda lime silica glasses. *Results Phys.* **2016**, *6*, 640–644. [[CrossRef](#)]

15. Naeimi, A.; Arabi, A.M.; Merajifar, V. A novel approach to the synthesis of Zn₂SiO₄: Mn luminescent nanoparticles. *J. Mater. Sci. Mater. Electron.* **2019**, *30*, 9123–9132. [[CrossRef](#)]
16. Svetlichnyi, V.; Shabalina, A.; Lapin, I.; Goncharova, D.; Nemoykina, A. ZnO nanoparticles obtained by pulsed laser ablation and their composite with cotton fabric: Preparation and study of antibacterial activity. *Appl. Surf. Sci.* **2016**, *372*, 20–29. [[CrossRef](#)]
17. Othman, Z.J.; Matoussi, A. Morphological and optical studies of zinc oxide doped MgO. *J. Alloys Compd.* **2016**, *671*, 366–371. [[CrossRef](#)]
18. Xie, J.; Cao, Y.; Jia, D.; Li, Y.; Wang, Y. Solid-state synthesis of Y-doped ZnO nanoparticles with selective-detection gas-sensing performance. *Ceram. Int.* **2016**, *42*, 90–96. [[CrossRef](#)]
19. Kumar, H.; Rani, R. Structural and optical characterization of ZnO nanoparticles synthesized by microemulsion route. *Int. Lett. Chem. Phys. Astron.* **2013**, *14*, 26–36. [[CrossRef](#)]
20. Essalah, G.; Kadim, G.; Jabar, A.; Masrouf, R.; Ellouze, M.; Guermazi, H.; Guermazi, S. Structural, optical, photoluminescence properties and Ab initio calculations of new Zn₂SiO₄/ZnO composite for white light emitting diodes. *Ceram. Int.* **2020**, *46*, 12656–12664. [[CrossRef](#)]
21. Elhadi, S.E.; Liu, C.; Zhao, Z.; Li, K.; Zhao, X. Structure and optical properties of ZnO/Zn₂SiO₄ composite thin films containing Eu³⁺ ions. *Thin Solid Films* **2018**, *668*, 1–8. [[CrossRef](#)]
22. Ramakrishna, P.V.; Murthy, D.B.R.K.; Sastry, D.L. White-light emitting Eu³⁺ co-doped ZnO/Zn₂SiO₄: Mn²⁺ composite microphosphor. *Spectrochim. Acta A Mol. Biomol. Spectrosc.* **2014**, *125*, 234–238. [[CrossRef](#)]
23. Omar, N.A.S.; Fen, Y.W.; Matori, K.A.; Zaid, M.H.M.; Norhafizah, M.R.; Nurzilla, M.; Zamratul, M.I.M. Synthesis and optical properties of europium doped zinc silicate prepared using low cost solid state reaction method. *J. Mater. Sci. Mater. Electron.* **2016**, *27*, 1092–1099. [[CrossRef](#)]
24. Copeland, T.S.; Lee, B.I.; Qi, J.; Elrod, A.K. Synthesis and luminescent properties of Mn²⁺-doped zinc silicate phosphors by sol-gel methods. *J. Lumin.* **2002**, *97*, 168–173. [[CrossRef](#)]
25. Xu, G.Q.; Xu, H.T.; Zheng, Z.X.; Wu, Y.C. Preparation and characterization of Zn₂SiO₄: Mn phosphors with hydrothermal methods. *J. Lumin.* **2010**, *130*, 1717–1720. [[CrossRef](#)]
26. Alibe, I.M.; Matori, K.A.; Yaakob, Y.; Rashid, U.; Alibe, A.M.; Zaid, M.H.M.; Nasir, S.; Nasir, M.M. Effects of polyvinylpyrrolidone on structural and optical properties of willemite semiconductor nanoparticles by polymer thermal treatment method. *J. Therm. Anal. Calorim.* **2019**, *136*, 2249–2268. [[CrossRef](#)]
27. Salem, A.; Saion, E.; Al-Hada, N.M.; Kamari, H.M.; Shaari, A.H.; Radiman, S. Simple synthesis of ZnSe nanoparticles by thermal treatment and their characterization. *Results Phys.* **2017**, *7*, 1175–1180. [[CrossRef](#)]
28. Baqer, A.A.; Matori, K.A.; Al-Hada, N.M.; Shaari, A.H.; Kamari, H.M.; Saion, E.; Chyi, J.L.Y.; Abdullah, C.A.C. Synthesis and characterization of binary (CuO)_{0.6}(CeO₂)_{0.4} nanoparticles via a simple heat treatment method. *Results Phys.* **2018**, *9*, 471–478. [[CrossRef](#)]
29. Naseri, M.G.; Saion, E.B.; Ahangar, H.A.; Hashim, M.; Shaari, A.H. Simple preparation and characterization of nickel ferrite nanocrystals by a thermal treatment method. *Powder Technol.* **2011**, *212*, 80–88. [[CrossRef](#)]
30. Al-Hada, N.M.; Saion, E.B.; Shaari, A.H.; Kamarudin, M.A.; Flaifel, M.H.; Ahmad, S.H.; Gene, S.A. A facile thermal-treatment route to synthesize ZnO nanosheets and effect of calcination temperature. *PLoS ONE* **2014**, *9*, 103134. [[CrossRef](#)]
31. Lee, P.J.; Saion, E.; Al-Hada, N.M.; Soltani, N. A simple up-scalable thermal treatment method for synthesis of ZnO nanoparticles. *Metals* **2015**, *5*, 2383–2392. [[CrossRef](#)]
32. Alibe, I.M.; Matori, K.A.; Saion, E.; Alibe, A.M.; Zaid, M.H.M.; Engku, E.G. A facile synthesis of amorphous silica nanoparticles by simple thermal treatment route. *Dig. J. Nanomater. Biostruct* **2016**, *11*, 1155–1164.
33. Alibe, I.M.; Matori, K.A.; Aziz, S.H.A.; Yazid, Y.; Saion, E.; Alibe, A.M.; Zaid, M.H.M.; Ghapur Engku, E.A.A.; Zangina, T. The Influence of Calcination Temperature on Structural and Optical properties of ZnO-SiO₂ Nanocomposite by Simple Thermal Treatment Route. *Arch. Metall. Mater.* **2018**, *63*, 539–545.
34. Engku Ali, E.A.G.; Matori, K.A.; Saion, E.; Aziz, S.; Zaid, M.H.M.; Alibe, I.M. Calcination effect to the physical and optical properties of Zn₂SiO₄ composite prepared by impregnation of ZnO on SiO₂ amorphous nanoparticles. *MS&E* **2018**, *440*, 012036.
35. Alibe, I.M.; Matori, K.A.; Saion, E.; Ali, A.M.; Zaid, M.H.M. The influence of calcination temperature on structural and optical properties of ZnO nanoparticles via simple polymer synthesis route. *Sci. Sinter.* **2017**, *49*, 263–275. [[CrossRef](#)]
36. Parhi, P.; Manivannan, V. Novel microwave initiated synthesis of Zn₂SiO₄ and MCrO₄ (M = Ca, Sr, Ba, Pb). *J. Alloys Compd.* **2009**, *469*, 558–564. [[CrossRef](#)]
37. Krsmanović, R.M.; Antić, Ž.; Mitrić, M.; Dramićanin, M.D.; Brik, M.G. Structural, spectroscopic and crystal field analyses of Ni²⁺ and Co²⁺ doped Zn₂SiO₄ powders. *Appl. Phys. A* **2011**, *104*, 483–492. [[CrossRef](#)]
38. Babu, B.C.; Rao, B.V.; Ravi, M.; Babu, S. Structural, microstructural, optical, and dielectric properties of Mn²⁺: Willemite Zn₂SiO₄ nanocomposites obtained by a sol-gel method. *J. Mol. Struct.* **2017**, *1127*, 6–14. [[CrossRef](#)]
39. Singh, V.; Prasad, A.; Deopa, N.; Rao, A.S.; Jung, S.; Singh, N.; Rao, J.L.; Lakshminarayana, G. Luminescence features of Mn²⁺-doped Zn₂SiO₄: A green color emitting phosphor for solid-state lighting. *Optik* **2021**, *225*, 165715. [[CrossRef](#)]
40. Diao, C.C.; Yang, C.F.; Wang, R.L.; Lin, J.J.; Fu, M.Y. Prepare high efficiency Mn²⁺-doped Zn₂SiO₄ green phosphors in air using nano-particles. *J. Lumin.* **2011**, *131*, 915–920. [[CrossRef](#)]

41. Babu, B.C.; Buddhudu, S. Emission spectra of Tb^{3+} : Zn_2SiO_4 and Eu^{3+} : Zn_2SiO_4 sol-gel powder phosphors. *J. Spectrosc. Dyn.* **2014**, *4*, 1–8.
42. Mohd Zaid, M.H.; Amin Matori, K.; Abdul Aziz, S.H.; Kamari, H.M.; Mat Yunus, W.M.; Abdul Wahab, Z.; Samsudin, N.F. Fabrication and crystallization of ZnO-SLS glass derived willemite glass-ceramics as a potential material for optics applications. *J. Spectrosc.* **2016**, *2016*, 1–7. [[CrossRef](#)]
43. Molla, A.R.; Tarafder, A.; Karmakar, B. Synthesis and properties of glasses in the $K_2O-SiO_2-Bi_2O_3-TiO_2$ system and bismuth titanate ($Bi_4Ti_3O_{12}$) nano glass-ceramics thereof. *J. Mater. Sci.* **2011**, *46*, 2967–2976. [[CrossRef](#)]
44. Pal, M.; Pal, U.; Jiménez, J.M.G.Y.; Pérez-Rodríguez, F. Effects of crystallization and dopant concentration on the emission behavior of TiO_2 : Eu nanophosphors. *Nanoscale Res. Lett.* **2012**, *7*, 1–12. [[CrossRef](#)] [[PubMed](#)]
45. Omri, K.; Lemine, O.M.; El Mir, L. Mn doped zinc silicate nanophosphor with bifunctionality of green-yellow emission and magnetic properties. *Ceram. Int.* **2017**, *43*, 6585–6591. [[CrossRef](#)]
46. Babu, B.C.; Buddhudu, S. Analysis of structural and electrical properties of Ni^{2+} : Zn_2SiO_4 ceramic powders by sol-gel method. *J. Sol-Gel Sci. Technol.* **2014**, *70*, 405–415. [[CrossRef](#)]
47. Babu, B.C.; Naresh, V.; Prakash, B.J.; Buddhudu, S. Structural, thermal and dielectric properties of lithium zinc silicate ceramic powders by sol-gel method. *Ferroelectr. Lett. Sect.* **2011**, *38*, 114–127. [[CrossRef](#)]
48. Ali, E.A.G.E.; Matori, K.A.; Saion, E.; Ab Aziz, S.H.; Zaid, M.H.M.; Alibe, I.M. Effect of sintering temperatures on structural and optical properties of ZnO- Zn_2SiO_4 composite prepared by using amorphous SiO_2 nanoparticles. *J. Aust. Ceram. Soc.* **2019**, *55*, 115–122.
49. Ali, E.E.; Matori, K.A.; Saion, E.; Aziz, S.H.A.; Zaid, M.H.M.; Alibe, I.M. Structural and optical properties of heat treated Zn_2SiO_4 composite prepared by impregnation of ZnO on SiO_2 amorphous nanoparticles. *ASM Sci. J.* **2018**, *11*, 75–85.
50. Omar, N.A.S.; Fen, Y.W.; Matori, K.A.; Aziz, S.H.A.; Alassan, Z.N.; Samsudin, N.F. Development and characterization studies of Eu^{3+} -doped Zn_2SiO_4 phosphors with waste silicate sources. *Procedia Chem.* **2016**, *19*, 21–29. [[CrossRef](#)]
51. Masjedi-Arani, M.; Salavati-Niasari, M. A simple sonochemical approach for synthesis and characterization of Zn_2SiO_4 nanostructures. *Ultrason. Sonochem.* **2016**, *29*, 226–235. [[CrossRef](#)]
52. Hashem, M.; Saion, E.; Al-Hada, N.M.; Kamari, H.M.; Shaari, A.H.; Talib, Z.A.; Paiman, S.B.; Kamarudeen, M.A. Fabrication and characterization of semiconductor nickel oxide (NiO) nanoparticles manufactured using a facile thermal treatment. *Results Phys.* **2016**, *6*, 1024–1030. [[CrossRef](#)]
53. Tarafder, A.; Molla, A.R.; Dey, C.; Karmakar, B. Thermal, Structural, and Enhanced Photoluminescence Properties of Eu^{3+} -doped Transparent Willemite Glass-Ceramic Nanocomposites. *J. Am. Ceram. Soc.* **2013**, *96*, 2424–2431. [[CrossRef](#)]
54. Omar, N.A.S.; Fen, Y.W.; Matori, K.A. Europium doped low cost Zn_2SiO_4 based glass ceramics: A study on fabrication, structural, energy band gap and luminescence properties. *Mater. Sci. Semicond. Process.* **2017**, *61*, 27–34. [[CrossRef](#)]
55. Lourenco, S.A.; Dantas, N.O.; Serqueira, E.O.; Ayta, W.E.F.; Andrade, A.A.; Filadelpho, M.C.; Sampaio, J.A.; Bell, M.J.V.; Pereira-da-Silva, M.A. Eu^{3+} photoluminescence enhancement due to thermal energy transfer in Eu_2O_3 -doped $SiO_2-B_2O_3-PbO_2$ glasses system. *J. Lumin.* **2011**, *131*, 850–855. [[CrossRef](#)]
56. Alibe, I.M.; Matori, K.A.; Sidek, H.A.A.; Yaakob, Y.; Rashid, U.; Alibe, A.M.; Mohd Zaid, M.H.; Ahmad Khiri, M.Z. Effects of calcination holding time on properties of wide band gap willemite semiconductor nanoparticles by the polymer thermal treatment method. *Molecules* **2018**, *23*, 873. [[CrossRef](#)] [[PubMed](#)]
57. Gao, X.D.; Li, X.M.; Yu, W.D. Synthesis and optical properties of ZnO nanocluster porous films deposited by modified SILAR method. *Appl. Surf. Sci.* **2004**, *229*, 275–281. [[CrossRef](#)]
58. Chen, H.; Ding, J.; Guo, W.; Chen, G.; Ma, S. Blue-green emission mechanism and spectral shift of Al-doped ZnO films related to defect levels. *RSC Adv.* **2013**, *3*, 12327–12333. [[CrossRef](#)]
59. Zeng, H.; Duan, G.; Li, Y.; Yang, S.; Xu, X.; Cai, W. Blue Luminescence of ZnO nanoparticles based on non-equilibrium processes: Defect origins and emission controls. *Adv. Funct. Mater.* **2010**, *20*, 561–572. [[CrossRef](#)]
60. Renitta, A.; Vijayalakshmi, K. Highly sensitive hydrogen safety sensor based on Cr incorporated ZnO nano-whiskers array fabricated on ITO substrate. *Sens. Actuators B Chem.* **2016**, *237*, 912–923. [[CrossRef](#)]
61. Yawalkar, M.M.; Nair, G.B.; Zade, G.D.; Dhoble, S.J. Effect of the synthesis route on the luminescence properties of Eu^{3+} activated $Li_6M(BO_3)_3$ ($M = Y, Gd$) phosphors. *Mater. Chem. Phys.* **2017**, *189*, 136–145. [[CrossRef](#)]
62. Đačanin, L.; Lukić, S.R.; Petrović, D.M.; Nikolić, M.; Dramićanin, M.D. Judd-Ofelt analysis of luminescence emission from Zn_2SiO_4 : Eu^{3+} nanoparticles obtained by a polymer-assisted sol-gel method. *Phys. B Condens. Matter.* **2011**, *406*, 2319–2322. [[CrossRef](#)]
63. Chen, P.; Ma, X.; Yang, D. ZnO: Eu thin-films: Sol-gel derivation and strong photoluminescence from $^5D_0 \rightarrow ^7F_0$ transition of Eu^{3+} ions. *J. Alloys Compd.* **2007**, *431*, 317–320. [[CrossRef](#)]
64. Golja, D.R.; Dejene, F.B. Effect of Eu^{3+} ion concentration on the structural and photoluminescence properties of $Ba_{1.3}Ca_{0.7}SiO_4$ ceramic-based red phosphors for solid-state lighting applications. *J. Alloys Compd.* **2020**, *827*, 154216. [[CrossRef](#)]
65. Basavaraj, R.B.; Nagabhushana, H.; Prasad, B.D.; Sharma, S.C.; Prashantha, S.C.; Nagabhushana, B.M. A single host white light emitting Zn_2SiO_4 : Re^{3+} (Eu, Dy, Sm) phosphor for LED applications. *Optik* **2015**, *126*, 1745–1756. [[CrossRef](#)]
66. Xie, X.; Chen, J.; Song, Y.; Zhou, X.; Zheng, K.; Zhang, X.; Shi, Z.; Zou, H.; Sheng, Y. Zn_2SiO_4 : Eu^{3+} micro-structures: Controlled morphologies and luminescence properties. *J. Lumin.* **2017**, *187*, 564–572. [[CrossRef](#)]

-
67. Zhang, H.X.; Buddhudu, S.; Kam, C.H.; Zhou, Y.; Lam, Y.L.; Wong, K.S.; Ooi, B.S.; Ng, S.L.; Que, W.X. Luminescence of Eu^{3+} and Tb^{3+} doped Zn_2SiO_4 nanometer powder phosphors. *Mater. Chem. Phys.* **2001**, *68*, 31–35. [[CrossRef](#)]
 68. Gupta, S.K.; Ghosh, P.S.; Sahu, M.; Bhattacharyya, K.; Tewari, R.; Natarajan, V. Intense red emitting monoclinic LaPO_4 : Eu^{3+} nanoparticles: Host–dopant energy transfer dynamics and photoluminescence properties. *RSC Adv.* **2015**, *5*, 58832–58842. [[CrossRef](#)]